CrossMark

ORIGINAL PAPER

Superconductor Stability Against Quench and Its Correlation with Current Propagation and Limiting

Harald Reiss[1]

Abstract This paper presents a numerical (finite element) analysis of superconductor stability and current propagation under random variations of critical superconductor parameters. Instead of using singular (homogeneous) values, random variations potentially are appropriate to take into account any conductor inhomogeneity that can be considered as an obstacle to current propagation. Traditional assumptions like homogeneous current distribution, critical temperature, critical current density and critical magnetic fields are not justified in general; a local disturbance (for example, release of mechanical stress energy), if not immediately distributed by solid conduction, would generate a transient increase of local conductor temperature. Local critical current density and magnetic field then will be reduced, and current distribution will change. Disturbances may arise also from transport currents that locally exceed the critical current of the superconductor. Disturbances of all kinds may increase the conductor temperature above its critical value. A local analysis of all superconductor states thus is mandatory to safely avoid a quench. As an extension of standard stability models, also flux flow resistive states are taken into account. We will try to find a possibly existing correlation between current propagation and superconductor stability. Fault current limiting is discussed as a special case of current propagation. The analysis is applied to a bundle of high-temperature superconductor (HTSC) filaments. As will be shown, temperature profiles in a superconductor do not allow a clear distinction between Ohmic resistive or flux flow resistive fault current limiting. Though frequently made in the literature, this separation is highly questionable, because Ohmic resistive and flux flow resistive states may locally coexist, side by side, but are not very stable in the superconductor volume.

1 Survey

A superconductor is stable if it does not quench. Quench is initiated by disturbances like insufficient cooling, local release of mechanical energy, absorption of particle radiation or transport currents exceeding the critical current. Quench proceeds on very small timescales. In many cases, quench causes local damage but may even lead to total destruction of a conductor. Quench can be avoided by appropriate design of superconductors (wires, filaments, thin films) using stability models. Stability models yield predictions on permissible conductor geometry like maximum radius of filaments or aspect ratio of thin films, and of maximum zero-loss transport current to which a superconductor may be exposed.

But fast transitions from superconducting to normal conducting state, like in a quench, offer rich potential of self-regulating fault current limiting (FCL), for example in case of short circuits in an electrical distribution system. When simulating current propagation, we accordingly have to consider two mutually exclusive situations: energy losses and quench during nominal conductor operation safely has to be avoided, which means the actual conductor temperature, current density and magnetic field have safely to be kept

✉ Harald Reiss
harald.reiss@physik.uni-wuerzburg.de

[1] Department of Physics, University of Wuerzburg, Am Hubland, 97074 Wuerzburg, Germany

🖄 Springer

below their critical values. On the other hand, fault current limiting relies just on overrunning the critical parameters. Simulation of current propagation has to account for both situations.

Attempts to develop FCL and successful realisations of this advanced safety concept have very frequently been reported in the literature and are an important step forward. Summary reports prepared soon after the discovery of high-temperature superconductivity, with reference to FCL projects, can be found in [1, 2]; a more recent description, again with numerous citations to original literature, is given in [3], Chap. 8. Design and successful operation of fault current limiters contribute to a deeper understanding of current transport in general and to short-time, superconductor materials behaviour under extreme current load.

Current limitation can be achieved if at least one of the three critical parameters (temperature T_{Crit}, critical magnetic field B_{Crit} and critical current density J_{Crit}) is exceeded by actual values T, B and J. Roughly speaking, an Ohmic resistive FCL integrated into an electrical circuit immediately after the start of a fault like $J >> J_{Crit}$ generates flux flow resistances and corresponding losses which quickly raise the conductor temperature to above T_{Crit}; thus, a large obstacle to fault current flow is generated. A flux flow FCL, too, generates flux flow resistance but with the conductor temperature below T_{Crit} (no phase change to normal conduction). Inductive current limiters comprise a primary normal conductor winding and a shielded iron core. Shielding of the core is realised by a secondary superconductor winding (a cylinder positioned between the primary conductor and iron core). Shielding is lost when large fault currents quench the superconductor, which in turn increases the impedance of the primary circuit.

Technically realised FCL are purposefully designed to suppress fault current in a medium voltage grid to tolerable residual values, preferentially to only a very small multiple of nominal current. In the past, there were about ten industrial, FCL projects of resistive and saturated iron core types, and there are about five projects at present.

The major idea of this paper is fourfold: (a) show that there is inhomogeneity of temperature and, as a consequence, of current distribution, critical temperature, current density, magnetic field and also of current limitation (because limitation might occur in only part of the cross section); (b) explain that a distinction between (solely) Ohmic resistive and flux flow resistive current limiting, as is presently done in the literature, becomes highly questionable; (c) introduce random critical parameters as a new method to account for shortages in materials development and manufacture issues; and (d) investigate possibly existing correlations between stability and current limiting.

Current limiters in this paper serve as extreme cases of current propagation. But focus is on the physics behind current propagation. We will describe by numerical methods how fast and to which extent a superconductor bundle reacts to a sudden increase of current load (like in a fault).

Investigations of current propagation and limiting that rely on homogeneous temperature distribution in the conductor cross section have been presented, e.g. in [3–5]; there are more numerous reports that apply the same simplifying assumption. But there are another four shortages of traditional stability models:

(a) The models assume instantaneous distribution within the conductor volume, or thermalisation, of a local disturbance.
(b) The models do not specify the location and intensity of a disturbance in the conductor.
(c) The Stekly, adiabatic or dynamic stability models derive results under quasi-stationary and adiabatic conditions; for a survey, see Wilson [6] or Dresner [7].
(d) Flux flow resistive states are not included.

Among these, items (a), (b) and (d) are the most critical ones. To improve the situation, standard stability models have recently been extended by numerical models (Flik and Tien [8], and by the present author). We have investigated the reaction of superconductors under *direct current (DC)* transport to either

(i) Transient disturbances [9]—a single (Dirac) heat pulse locally released in the conductor by absorption of infrared or particle radiation, or by a sudden transformation of mechanical to thermal energy (conductor movement under Lorentz forces)
(ii) Periodic disturbances [10, 11]—exposure of a sample to periodic energy pulses that as local disturbances lead to periodic variations of local temperature and corresponding, periodic variations of critical current density and stability functions

Investigations in [8–11] apply the temperature dependency of the critical current density as the sole basis to predict the maximum zero-loss transport current by a stability function (this function is explained later). The investigations have not considered losses that may arise under flux flow resistive states ($J > J_{Crit}$), with the conductor temperature below the critical temperature.

A very interesting case (iii) accordingly appears when the density of an *alternating current (AC) itself* initiates periodic disturbances by flux flow losses. The disturbances then are no longer point-like, isolated from each other or of only a very short duration, but may be extended over a considerable part (or total) of the conductor cross section. They also may oscillate and exist over extended periods of time. This case will be studied in this paper.

The paper is organised as follows: In part I, a numerical model will be described to calculate local electrical, magne-

tic and thermal states of a high-temperature superconductor (HTSC) under disturbances initiated by a transport or a fault current. The simulations are applied to a bundle of several hundred identical conductor filaments all switched in parallel (the selection of a HTSC *model* conductor material is in detail explained in Appendix A1). The bundle is integrated into an electrical circuit (Fig. 1a) that allows comparison with a similar system described in [4] with same root mean square phase voltage, same conductor cross section and same critical current density. We could in principle take any large- or small-scale electrical grid, like in a laboratory experiment, with an appropriately dimensioned superconducting component; the point is the analysis of this component under high current load.

Figure 1a also incorporates a normal conductor with non-zero resistance (in a large-scale experimental setup, the normal conductor in Fig. 1a might be a conventional transmission line or a standard power cable). The resistance of
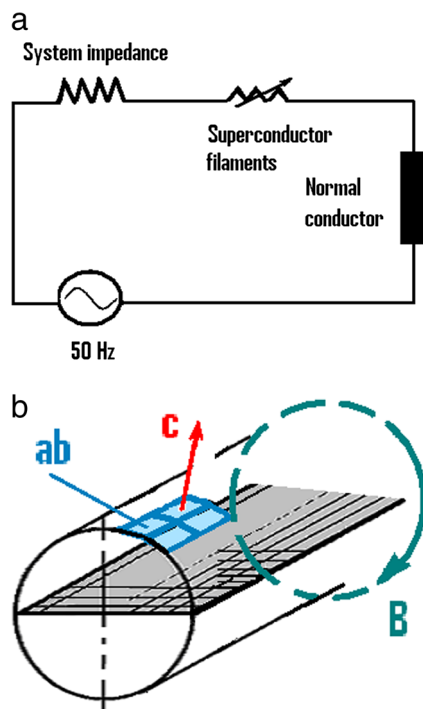
Fig. 1 a Schematic view of an electrical grid. A sudden, strong increase of current load onto a superconductor filament bundle will be simulated, either in a small-scale laboratory experiment or, on large scale, the grid could describe a medium voltage distribution system. The normal conductor serves as an auxiliary variable; its assumed sudden decrease initiates the increase of transport current (not necessarily a fault caused by accidents like short circuit or lightning). **b** Schematic view, not to scale, showing an axial section of a superconductor filament (polycrystalline material) embedded in a metallic matrix (not shown). Current direction is parallel to longitudinal axis of symmetry. The figure assumes ideal c-axis orientation of grains (*light blue*; size strongly enlarged) and circumferential direction of the magnetic field (flux density; *green circle*). The *flat grey surface* illustrates the finite element scheme of 4-node, plane model elements which are rotated against the longitudinal axis to generate volume elements

this conductor, and thus the total resistance of the circuit, is used as an auxiliary variable: Continuous, though fast, reduction of the resistance serves for definition of a sudden strong increase of transport current, a procedure that strongly simplifies numerical calculations and stabilises the achieved solutions.

Part II of the paper reports results for integral conductor states like stability functions, maximum zero-loss currents and current limiting. Part III deals with a possible correlation between stability, current propagation and limitation.

2 Description of Stability, Current Propagation and Limiting Calculations

The numerical concept (meshing, boundary conditions, solution schemes) originates from a finite element method (Reiss and Troitsky [12]) how to obtain thermal diffusivity of opaque, transparent or semitransparent thin films; an analogue of this procedure recently has been applied [9–11] to the investigation of superconductor stability.

2.1 Data Input

Electrical resistances of the superconductor filaments comprise Ohmic, inductive, flux flow, hysteresis and coupling resistances (the filaments shall be embedded in a metallic matrix). Dimensions of the filaments, details of meshing and solution schemes will be reported in Section 2.4.

Strictly speaking, we could take any reasonable superconductor material for stability analysis (reasonable in the sense that it allows numerical, finite element simulations to converge). This requests, for example, that the critical temperature of the conductor is not 10^{-6} K or the like, or its anisotropy is not in the order of 10^3. In principle, even an LHe-cooled LTSC could be applied and also any conductor architecture. Results like existence of transient temperature profiles, large temperature gradients, local current distribution and an anticipated correlation between stability and current propagation and suppression, *qualitatively* were the same. However, the computational problems were much larger, and convergence of the results might be impossible to obtain.

The numerical simulations thus have to be performed with a simple conductor architecture and a HTSC material (as mentioned, a model conductor) of which its electrical/magnetic and thermal properties shall be available from experiments, over a large range of temperature and, according to experience, its anisotropy to current transport be modest (in the order of 10; this is fulfilled with a YBaCuO solid).

The application of a model conductor, as will be shown, clearly illustrates the problems that would arise in *any* 1G or

2G conductor under transient current propagation (the problems reflect the list of major ideas of this paper, as given in Section 1): inhomogeneity of temperature and current distribution; inhomogeneity of critical temperature, current density and magnetic field; and inhomogeneity of current limitation.

All parameters of the conductor take into account interactive physical dependencies, like T_{Crit} vs. $B_{Crit1,2}$, or $B_{Crit1,2}$ vs. T, and thermal diffusivity vs. T.

Modelling of Ohmic resistance states is straight-forward with data from [13], and modelling of flux flow resistivity to axial current (Fig. 1b) is made according to [14]. The weak-link structure of a polycrystalline conductor constitutes a potential obstacle that is laid upon is constituents; the obstacle not only concerns electrical transport (electron charges) but also magnetic (movement of vortices under flux flow) and thermal transport. Resistance to magnetic transport has to be considered separately in grains and in grain boundaries. A schematic, rather optimistic orientation of plate-like grains and circumferential magnetic field, under axial current, is indicated in Fig. 1b (small, light-blue shells). Flux flow, if any, roughly occurs in radial directions only.

Reference [14] explains that the low temperature, empirical relation between specific resistivity of flux flow, ρ_{FF}, and normal conduction, ρ_{NC}

$$\rho_{FF} = \rho_{NC}B/B_{Crit,2} \qquad (1)$$

is applicable to also high-temperature superconductors. However, this relation is valid for superconductor *solids*, and as [15], p. 128, points out, there may be deviations from (1) in type II superconductors (like HTSC) with large values of the Ginzburg-Landau parameter, κ; this accordingly could indicate a problem in the present study but will not be pursued here. Instead, in the present simulations, the overall structure of (1) shall be maintained but modifications applied to account for weak-link behaviour.

References [12] and [14] report strong anisotropy of the resistance against transport of magnetic flux vortices, much larger than anisotropy of resistance to current. In a rough approximation, we have estimated grain and grain boundary volumes and the results used as weights assigned to the anisotropy ratios that were estimated following [14, 16]. A weighted mean accounting for porosity and anisotropy is applied as a pre-factor to (1). Details of the procedure will be reported elsewhere.

The final result, axial resistivity, ρ_{FF}, to current transport, under radial flux flow in the porous, polycrystalline, roughly layered material, is shown in Fig. 2. The resistivity ρ_{FF} is larger than ρ_{NC}, contrary to what would be expected from the standard (1). But (1), in its original form, applies to *solids*, not to a network of solid particles surrounded by weak-link shells; the comparatively large ρ_{FF} thus does not necessarily indicate strong flux pinning. The resistivity ρ_{FF}
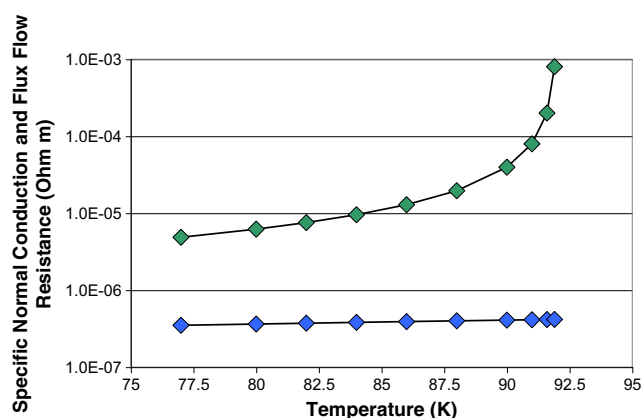
Fig. 2 Specific resistance to transport current under normal conduction (*blue diamonds*) and to flux flow (*green diamonds*) in *porous* YBaCuO, vs. temperature, at magnetic flux densities that exceed the lower critical field, $B_{Crit,1}$. The large difference results from estimated contributions of grain boundaries (weak links) to flux flow resistance; for more explanations, see text

is also larger than the constant $\rho_{FF} = 10^{-6}$ Ω m used in [4]; it is not at all clear that ρ_{FF} should be constant, independent of temperature.

Thermal diffusivity, D_T, of a YBaCuO superconductor solid material (with conductivity from [17]) is between $4 \, 10^{-6}$ and $2 \, 10^{-6}$ m²/s, at temperatures of 77 and 120 K, respectively. The values are the same as previously used [9 - 11]; compare the original literature cited therein. For a periodic disturbance that initiates a local increase of temperature, and when taking a mean value of D_T in the expression for the penetration depth $\delta_{SC}(\omega) = C (2D_T/\omega)^{1/2}$ of a thermal wave ([18], p. 159), we have $\delta_{SC}(\omega) \approx 1600 \, \mu$m, with C a constant, for simplicity C = 4.6 for a flat, semi-infinite sample, and $\omega = 50$ Hz. Also, this estimate applies to a solid; it does not take into account the porosity of the conductor. However, a correction to D_T using the traditional Russell cell model (see below) does not yield substantial alterations so that $\delta_{SC}(\omega)$ safely exceeds r_{Fil}, the filament radius defined in Section 2.4. Local temperature, $T(x, y, t)$, of all volume elements in the filament thus will very quickly respond to any disturbance that propagates by thermal diffusion through the polycrystalline network but does not, as will be shown, guarantee a homogeneous conductor temperature.

Geometry and orientation of the grains (Fig. 1b) assume an ideal case, a layered distribution of platelets from which the more deviations will have to be expected, the more layers would be generated. To obtain both electrical resistivity and thermal conductivity of porous materials, the traditional Russell cell model is applied to the corresponding solid state data ([19]; an old but flexible model since it is applicable to particulates of rather arbitrary shape). We use porosity, $\Pi = 0.1$, of the superconductor material, and

for the linear part of the normal state resistivity, ρ_{NC}, the slope $d\rho_{NC}/dT = 4.27 \, 10^{-9}$ Ω m/K reported in [14]. For application of Russell's cell model, it is assumed that the resistivity against current transport in grain boundary volumes is by a factor of at least five larger than within grains. This ratio is a very rough estimate and not identical to, but much smaller than, anisotropy of transport of magnetic flux vortices.

Inductive losses of the filament bundle have been estimated following traditional models (standard electrotechnical literature) and do not need specification. Hysteresis and coupling losses are modelled following [6], Chap. 8.2 and 8.3. All losses, if they depend on current, can be transformed into expressions that contain corresponding specific electrical resistances. Corrections to the most important Ohmic and flux flow resistive losses by inductive, hysteresis and coupling counterparts are small.

Electrical and thermal properties of the matrix material are needed for description of current sharing (see the results in Appendix A2, Figs. 14, 15, 16 and 17).

A new concept introduced in this paper is consideration of critical current density, critical temperature, upper critical magnetic field and the weak-link problem overlaid onto flux flow transport as *random* variables:

No existing superconductor, if manufactured in technically important quantities, shows perfectly homogeneous materials properties. Deviations from ideal conditions must be taken into account that may arise during conductor design and manufacture. Conductor inhomogeneity may turn out, for example, as local deviation from oxygen stoichiometry, or may result from high angle grain boundaries as obstacles against current transport in basal planes, or from tolerances in mechanical working steps, or from weak links, in total a very large number of potential divergences arising in polycrystalline materials. Modelling their impact on current propagation using, like in radiative exchange calculations, cell models (for example, the well-known brick wall model) is too simplifying and could lead to enormous uncertainties. A possible way out of the problem is to treat the most important critical parameters as statistical quantities (random values, with fluctuations around their mean).

We have applied random values like those illustrated in Figs. 12 and 13 (Appendix A1). In this model, critical current density and the other critical parameters of the superconductor and its weak link, anisotropic resistance against flux flow, are different in *each* of the finite elements (but with the traditional dependency on field and temperature, respectively). Maximum fluctuation is roughly estimated from experience [22]. Application of this model seems plausible (though it introduces additional numerical problems), but general validity of this concept has to be verified in additional studies.

2.2 Overall Calculation Scheme

The overall numerical procedure consists of four steps:

(a) Calculation of transient temperature fields by a standard finite element method.
(b) Re-calculation of resistances and critical parameters.
(c) Determination of the new current distribution; comparison of conductor temperature, magnetic field and current with the corresponding critical ones; and re-calculation of resistances and losses.
(d) Specification of a fault (or, more generally, of a sudden, strong increase of current) and return to step (a); we will in the following simply speak of a fault although the simulated strong current increase might not reflect an accident like short circuit or lightning.

In step (a), we use the same data for boiling LN_2 as in previous reports [9 - 11]. Close to the interface to the coolant, oscillations of $T(x, y, t)$ against coolant temperature are small; maximum amplitude variation in the present study is within $\Delta T = 1$ K, which means there will be almost no periodic but approximately constant thermal boundary conditions at the solid/liquid interface. After an initial settling period needed for creation of the first nitrogen vapour bubbles (in the order of 5 ms), the static description of boiling heat transfer is applicable (we again take data reported for smooth metallic surfaces; compare the original literature cited in [9 - 11]).

In step (b), the Meissner effect has to be checked separately in each of the finite elements of the numerical calculation scheme. Its property, "zero resistance" at magnetic fields below the lower critical field, cannot be handled reasonably when in a transient numerical analysis current distribution shall be determined from Kirchhoff's laws. Very small but finite values of the specific resistances (values below 10^{-20} Ω m) then have to be assumed.

The resistances obtained in step (b) are the basis to determine the new transient current distribution in step (c). The new distribution not necessarily is the same as obtained in previous time steps; instead, the distribution may fluctuate and the current percolate through the conductor, all in dependence of the actual resistances.

Summation over all re-calculated local currents yields the same total current in the conductor cross section, at all axial positions of the conductor including the metallic matrix.

In step (d), it has been assumed that a strong increase of current is initialized, under the nominal voltage of the circuit, by a sudden but controlled reduction, within 2.5 ms, of the total AC resistance of the grid. As mentioned, this not necessarily indicates really a fault (in a small-scale example of Fig. 1a, a sudden current increase might result from cutting off a large normal resistance from a laboratory circuit);
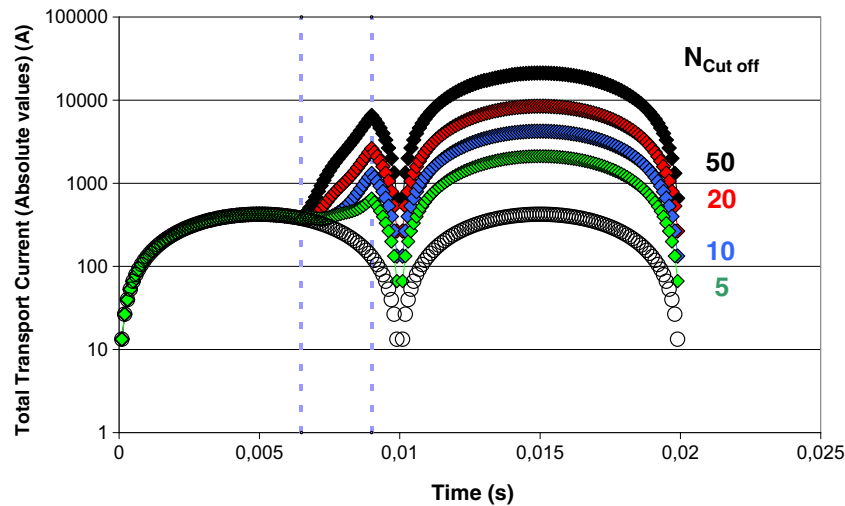
Fig. 3 Absolute value of total (nominal plus fault) current, $I_{Transp}(t)$, within $0 \leq t \leq 20$ ms (note the logarithmic ordinate scale). The figure shows to which extent the transport current will increase if the (AC) phase resistance, within $6.5 \leq t \leq 9$ ms, is reduced to $1/N_{Cut\,off}$ of its undisturbed value. The length of the normal conductor is 10^5 m, in order to keep the current load onto filaments small. *Open black circles*

denote the undisturbed normal conductor ($N_{Cut\,off} = 1$). Results are obtained with T_{Crit}, J_{Crit}, $B_{Crit,1}$ and $B_{Crit,2}$ *identical in each element* (not random numbers) and with the same field or temperature dependency, respectively, and constant anisotropy for transport of magnetic flux quanta. The local upturn of the curves is the stronger, the larger $N_{Cut\,off}$

the point is that the method shall generally be applicable, not only to public grids.

For this purpose, divisors, $N_{Cut\,off}$, beginning at $t = 6.5$ ms after the start of the simulation, gradually increase from an initial value, $N_{Cut\,off} = 1$, to their final value at t = 9 ms and then are constant. The $N_{Cut\,off}$ are used as auxiliary variables. No attempt was made to simulate details of a real short circuit like excursion of overcurrent and inductive voltage, $-L\ dI/dt$, at the position of the fault, temporarily existing arcs, resistances and their lifetimes.

Increase of the total (nominal plus fault) current (absolute value) is illustrated in Fig. 3 for different final $N_{Cut\,off}$. Note the upturn of all curves (coloured diamonds) during $6.5 \leq t \leq 9$ ms: Increase of the total current (under nominal voltage) by the reduced resistance to very large values overcompensates its reduction expected from the oscillation of nominal current, $I_{Transp}(t) = I_0 \ (\sin \omega t)$, during this period.

2.3 Solution Scheme

The total simulated period has been split into periods $\Delta t = 10^{-4}$ s. To obtain convergence of the results, the procedure within each period Δt had to be repeated by up to $N = 10$ iterations of steps (a) to (d) specified in Section 2.2. The large number of iterations reflects the strong nonlinearity of almost all involved parameters. Integration time δt within each Δt is between 10^{-14} and 10^{-7} s. Convergence is achieved at the end of each sub-step of duration

$\Delta t/N = 10^{-5}$ s. The calculations yield a series of converged, quasi-stationary solutions. This scheme generates convergence because the time interval $\Delta t/N$ is large in comparison to

(i) Characteristic (diffusion) time, τ_C, of electrical or magnetic fields and of currents, $\tau_C \leq 4\ r_{Fil}^2/(\pi^2\ D_C)$ ([6], p. 143) using for the diffusivity the expression $D_C = \rho_{NC}/\mu_0$, with ρ_{NC} the specific resistivity of the filament material in the normal conducting state, and μ_0 the vacuum constant. We have $D_C = 0.361$ m^2/s. This yields $\tau_C \leq 10^{-7}$ s.

(ii) Time τ_R needed to establish new equilibrium charge distributions (compare [21], Fig. 2b). This period covers total redistribution of electron pairs to the ground states of the superconductor; this would request also the exchange of charge between neighbouring elements. The estimates yield $\tau_R < 10^{-6}$ s except for temperatures very close to the critical temperature.

No divergences ($T < 77$ K, or runaway to an extremely high temperature) were finally observed that could result from too large a time step or from too small an element volume in the numerical procedure.

Both estimates (i) and (ii) justify calculation of the transient current distributions in a *stepwise* numerical procedure to obtain quasi-stationary, discrete intermediate states. If these conditions were not fulfilled, the procedure would have to be altered to a *continuous* model of current exchange between neighbouring finite elements to allow

re-organisation of charge distribution in the whole conductor, too difficult a task to be solved presently.

Computational efforts to fully cover all these procedures were enormous. The solution scheme applied sparse matrix direct solvers (requests a large memory space; alternatives like JCG or ICG iterative solvers were tested but convergence is not guaranteed). The calculation scheme (a) to (d), with in step (a) the embedded finite element core (a commercially available FE code), for simulation of a total period of 10 ms, took a standard PC with 4 GB workspace about 8 to 10 h, under Windows XP or Windows 7. This mainly results from the large number of IF…THEN…ELSE steps to be executed separately in each of the elements, with respect to all potentially allowed superconductor resistance states, and in each iteration cycle.

Nodal temperature results from solution of Fourier's differential equation. In the present case, 4-node, plane model elements have been applied, with rotation against the axis of symmetry to generate volume elements. Element temperature is the arithmetic mean of nodal temperatures.

2.4 Conductor Geometry and Critical Current Density

Finite element size is $\triangle r = 6 \ \mu m$ radial thickness and $200 \ \mu m$ axial length. The most inner elements are rods of circular cross section, whereas all other elements (superconductor and matrix) are circular shells (annuli of constant width).

Size of filaments in OPIT band-like (1G) conductors usually is about $20 \times 200 \mu m$. Current transport and temperature simulations in this fine structure would request too short characteristic and integration times. Instead, modelling of the conductor follows Wilson [6], Fig. 12.9, with a double or multi-stacking technique: We call a "filament" a composite of $1 < N_{thr} \leq N_{thr,max}$ very thin, superconductor threads (objects that result from extrusion). Definition of this filamentary composite (threads plus matrix) is for calculation purposes only; its radius is $r_{Fil} = 300 \mu m$. The conditions set for $\triangle r$ (radial width of finite elements), a_r (aspect ratio), r_{Fil} (filament radius) and Russelss cell model then allow modeling of the interior of one filament as a structural *continuum* (instead of explicitly modeling fine threads). The calculated results (inhomogeneity of temperature, etc. within one filament) do not depend on the filament (composite) radius r_{Fil}.

All filaments are bundled into a strand of identical filaments. A number $N_{Fil} = 354$ filaments yields total superconductor (bundle) cross section $A_{SC} = 10^{-4} m^2$, the value reported in [4]. The number N_{thr} of fine threads in the total (strand) cross section, $N_{Fil} < N_{thr} \leq N_{Fil} \times N_{thr,max}$, and the amount of weak link and metal matrix material are adjusted to yield filament (not strand) porosity $\Pi = 0.1$ to

be used in Russel' cell model [19]. The amount $1 - \Pi$ in one filament is occupied by the superconductor threads. The relative amount of superconductor material in one strand is much lower, like in LTSC strands.

The filaments are, in principle, of arbitrary length, $L_{Fil} >> r_{Fil}$. Before the start of the proper simulations, conductor length is limited to $L_{Fil} = L_{SC} = 500$ m; see below for this estimate.

We select one single filament to be simulated; it shall be located close to the periphery of the bundle (close to the solid/liquid interface to the coolant). Thickness of the metal matrix at peripheral positions is about 200 μm (larger than the clearance between filaments located in the interior of the strand).

Assume as a macroscopic example of Fig. 1a that the length of the normal conductor in Fig. 1a is $L_{Cu} = 12.5$ km and the impedance of one phase amounts to 0.38 Ω (same value as in [4]). With the specific resistance of Cu, $\rho_{Cu} = 1.8 \ 10^{-8} \ \Omega$ m, and a cross section $A_{Cu} = 10^{-4} \ m^2$ (again the same as in [4]), we have a loss of resistance of $\Delta R_{Cu} = 22.5 \ \Omega$ if the normal conductor resistance loss were total, $N_{Cut off} \rightarrow \infty$; this loss shall at least partly be compensated by the superconductor filament bundle. By its length and cross section, the resistance of the normal conductor determines the current load onto the superconductor filaments.

Assume for the moment that filament temperature is homogeneous and above critical temperature, say $T = 100$ K ($T_{Crit0} = 92$ K of YBaCuO), which means the filaments altogether would act as an Ohmic resistance current limiter. The specific resistance of the conductor at this temperature is about $\rho_{SC} = 4.5 \ 10^{-7} \ \Omega$ m. Length L_{SC} of the filaments then can be estimated from $\Delta R_{Cu} = \rho_{SC} \ L_{SC}/A_{SC}$, with the total cross section, A_{SC}, of the bundle of filaments. Using the said $A_{SC} = 10^{-4} \ m^2$, this yields the above-mentioned L_{SC} of about 500 m. Note that this simple estimate relies on a homogenous conductor temperature, $T = 100$ K, of all filaments, which, as we will show, is not the reality.

If only part of the filament cross sections would be in Ohmic resistance state (it will be shown below that this is indeed the case), or if the superconductor specific resistance is larger than the $\rho_{SC} = 4.5 \ 10^{-7} \ \Omega$ m, a strongly different, smaller L_{SC} could result. The L_{SC} of 500 m is of the same order of magnitude like the $L_{SC} = 232$ m reported in [4] for design of a flux flow current limiter.

In the following simulations, either number, N_{Fil}, of filaments or filament and normal conductor lengths, L_{SC} or L_{Cu}, respectively, *or* the critical current density, J_{Crit}, will be varied:

(a) $177 \leq N_{Fil} \leq 881$; $N_{Fil} = 354$ yields total conductor cross section $A_{SC} = 10^{-4} \ m^2$, again the value used in

[4]. In these tests, $L_{Cu} = 10^3$ m, $A_{Cu} = 10^{-4}$ m^2 and $L_{SC} = 500$ or 5000 m

(b) $10^2 \leq L_{Cu} \leq 10^5$ m; $N_{Fil} = 354$, $L_{SC} = 500$ or 5000 m, $A_{Cu} = 10^{-4}$ m^2 kept constant

The $L_{SC} = 5000$ m will be explained below. In the following cases (i) and (ii), "higher" and "lower" values of $J_{Crit}(T, B)$ are calculated from corresponding random reference values, J_{Crit0} (the higher J_{Crit0} are plotted in Fig. 13, Appendix A1).

Cases (i) and (ii) are defined as follows:

(i)   A mean value of $J_{Crit} = 3.75 \; 10^8$ A/m^2 at T = 77 K and magnetic field $B = 100$ mT. In text and figure captions, this value will be called the "higher" J_{Crit}.

(ii)   In order to replicate the results reported in [4], also a mean value of tentatively $J_{Crit} = 10^7$ A/m^2 is applied in the calculations (this is the "lower" J_{Crit} taken from [4]).

A field dependence of J_{Crit} was neglected in [4]. Random values of J_{Crit0} in the present calculations have been adjusted to replicate the 10^7 A/m^2, as a mean value, again at T = 77 K and $B = 100$ mT. This J_{Crit} is rather small; HTSC filaments with significantly higher J_{Crit} have become available which shall be accounted for by the higher J_{Crit}, case (i).

All calculations apply $N_{Cut\,off} = 20$ finally obtained at $t = 9$ ms (and then are kept constant); this limit is applied to interpret the results in a general sense and is not necessarily restricted to faults arising from accidents and in medium voltage grids only.

Except for the superconductor, the phase impedance (0.38 Ω) is the only resistance considered in [4] (they assume that no non-zero Ohmic resistance has survived the short circuit). In the present model, a length $L_{Cu} = 4.2 \; 10^4$ m of the normal conductor is required, under $N_{Cut\,off} = 20$, to replicate the absolute value of total phase resistance (the reported 0.38 Ω). When in the following figures length $L_{Cu} = 4.2 \; 10^4$ m of the normal conductor is indicated, it is done so to solely introduce an equivalent resistance of 0.38 Ω into the circuit.

Results obtained with the higher J_{Crit} in the following figures are identified by coloured solid or open symbols or black triangles. Light or dark grey symbols concern results calculated for the design described in [4] using the lower or higher J_{Crit}, respectively.

If there was *no* temperature dependence of J_{Crit} (but only a dependence on the local magnetic field), the transport current would flow in regions of the conductor cross section where the magnetic field is small, in the present case near the axis of symmetry. But this is not confirmed in reality. Both magnetic field distribution *and* temperature distribution are responsible, not only for the

local $J_{Crit}(x, y, t)$ but also for transport current distribution, $J(x, y, t)$.

With the given filament radius and the calculated filament current, local values of B(x,y,t) as expected are in the order 10^{-4} to 100 mT.

Random values of T_{Crit0} are shown in Fig. 14 (Appendix A1). They have to be converted to field-dependent $T_{Crit}(B)$, which is achieved with the corresponding inverse function derived from $B_{Crit}(T) = B_{Crit0}(1 - (T/T_{Crit})^2)$.

Both J_{Crit0} and T_{Crit0} are *materials* properties (randomly distributed in the cross section), while $J_{Crit}(T, B)$ and $T_{Crit}(B)$ are *conductor* properties because they reflect the actual operational states of the conductor, with the dependency on transient T and B; only these have to be considered in the numerical simulations and for calculation of stability functions.

Accordingly, to determine the transient resistive states of all parts of the conductor, the following relations have to be checked separately in each element:

$$T \leq T_{Crit}(B), \text{ with } T = T(x, y, t) \text{ and}$$
$$B = B(x, y, t), \text{ and} \tag{2a}$$
$$J_{Transp} \leq J_{Crit}(T, B), \text{ with } J_{Transp} = J_{Transp}(x, y, t),$$
$$T = T(x, y, t) \text{ and } B = B(x, y, t), \tag{2b}$$

3 Results

3.1 Temperature Fields

Figure 4a shows the calculated temperature field, T(x,y,t), in a section of 3.2 mm axial length of a single superconductor filament. It is not possible to simulate the current propagation problem over the whole length of filaments (for substantial limiting of fault current by flux flow resistances: at least hundreds of metres). Attempts to do so would not be very reasonable: We would immediately be driven back to simplifications like homogeneous conductor temperature and homogeneity of the other properties. If thermal contact between filament and matrix, and between matrix and coolant, remains the same over the whole length of a bundle containing a large number of filaments (an ideal situation but little speaks against it), the simulated short length is justified.

Results are presented at $t = 9$ ms after the start of the simulation for $L_{SC} = 232$ m, $L_{Cu} = 4.2 \; 10^4$ m, $N_{Fil} = 354$, $J_{Crit}(T = 77$ K, $B = 100$ mT$) = 10^7$ A/m^2 (mean value, the lower J_{Crit} that equals the J_{Crit} assumed in [4]). Temperate variation in this case is within only 0.5 K (compare the horizontal bar), in radial or axial directions within this short section. Provisionally, this speaks in favour of current limitation, if any, by flux flow resistance.

Fig. 4 **a** Temperature field in an axial section (3.2 mm length) of a filament conductor (the diagram is provided by the finite element code). The *horizontal bar* indicates the range of the calculated temperature. Results are given for t = 9 ms (the end of the increase of $N_{Cut\,off}(t)$) with $L_{SC} = 232$ m, $L_{Cu} = 4.2$ 10^4 m, $N_{Fil} = 354$ filaments and the *lower* J_{Crit} values (compare text; mean value J_{Crit} (T = 77 K, B = 100 mT) = 10^7 A/m^2). The calculation applies random values of T_{Crit}, J_{Crit} and $B_{Crit,2}$ and a divisor, $N_{Cut\,off} = 20$ (final value obtained at $t = 9$ ms). **b** Temperature field; same calculation as in Fig. 4a but with the *higher* J_{Crit} (compare text; mean value J_{Crit} (T = 77 K, B = 100 mT) = 3.75 10^8 A/m^2). Results are given for t = 9 ms. Note the regular variations of temperature observed at axial distances of about 600 μm that may develop to hot spots; they probably result from application of the random T_{Crit}, J_{Crit} and $B_{Crit,2}$ in the calculations (these variations are absent in Fig. 5)
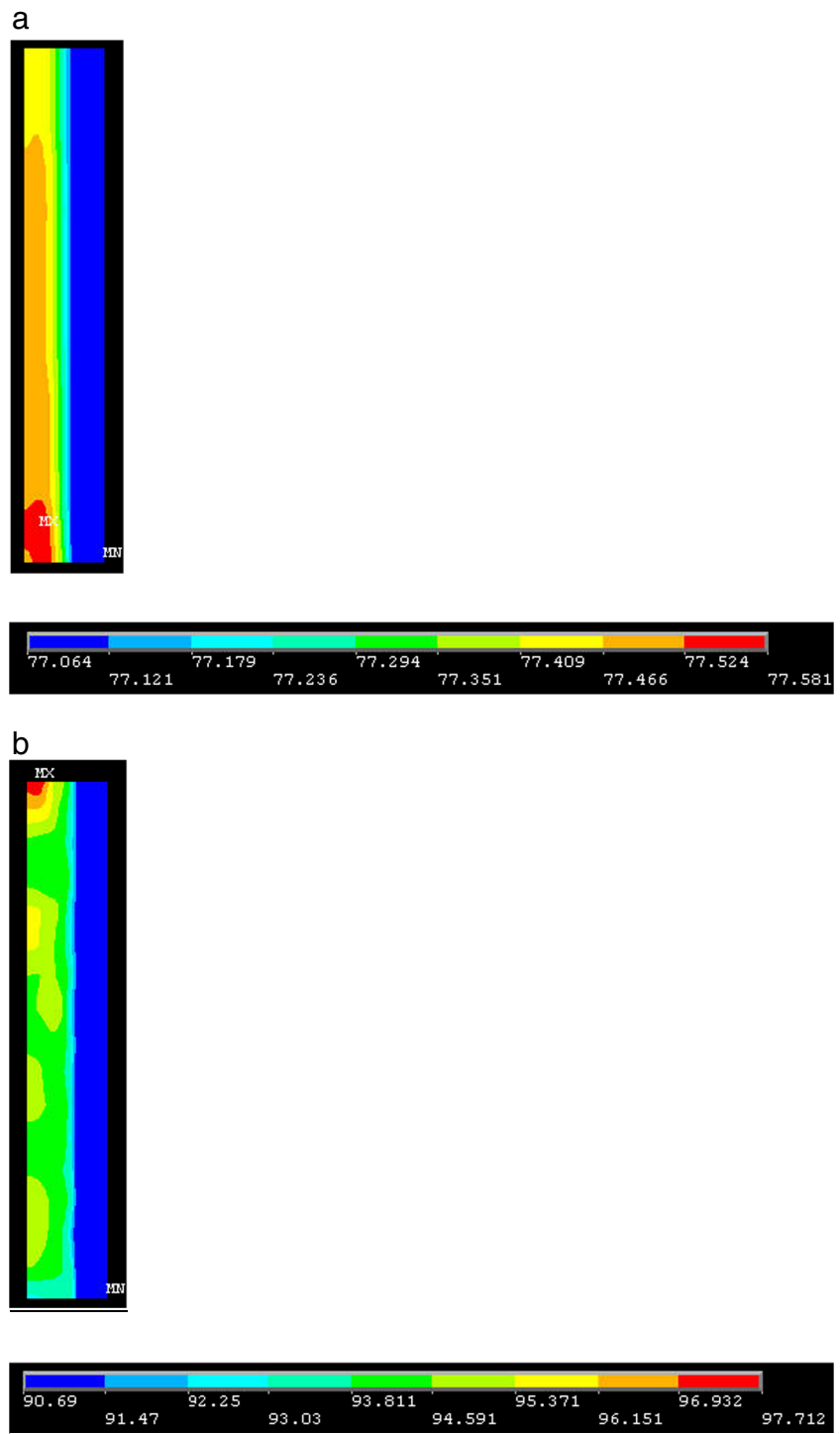
The situation changes significantly if instead of $J_{Crit} = 10^7$ A/m^2 a mean value $J_{Crit} = 3.75\ 10^8$ A/m^2 (the higher J_{Crit}) enters the calculations (Fig. 4b). No homogeneous temperature distribution, except within small regions close to and within the metallic matrix, can be identified: Instead, radial variation of conductor tempera-ture amounts to about 7 K. Accordingly, there are regions where $T(x, y, t)$ is below or, close to these regions, above the individual, randomly distributed critical temperatures. Current limitation, if any, thus would intuitively be expected from solely the corresponding local Ohmic resistances. But it is clear that a distinction between solely Ohmic

Fig. 5 Temperature field as in Fig. 4a, b; results have been obtained immediately before the start of the disturbance (t = 6.5 ms) using T_{Crit}, J_{Crit}, $B_{Crit,1}$ and $B_{Crit,2}$ *identical in each element* (no random numbers, but with corresponding temperature or field dependency, respectively). Note the homogeneous stratification of the temperature distribution within the superconductor filament
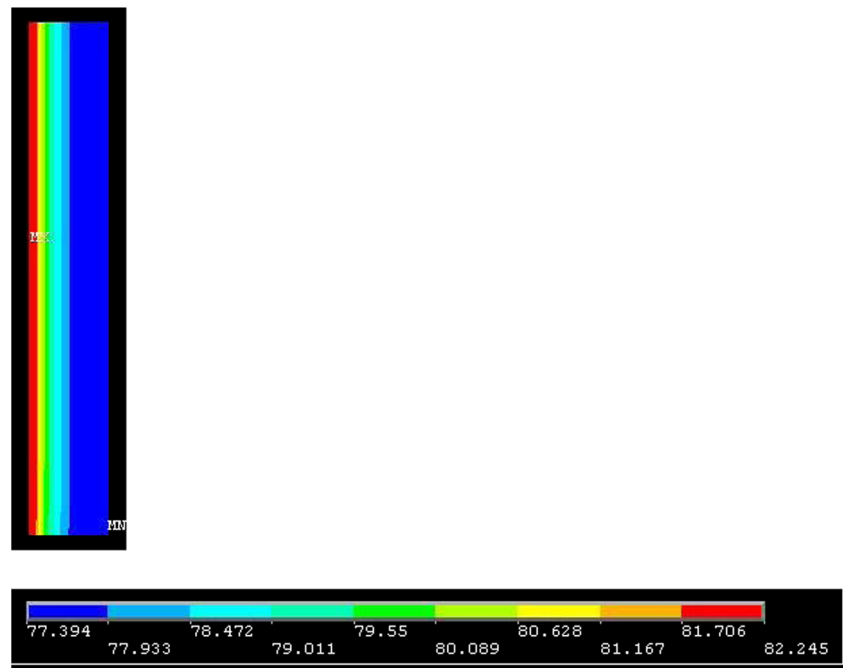

or solely flux flow resistive limiting of current propagation becomes questionable if there are temperature profiles, with temperature variations of this magnitude, in a conductor.

Both Fig. 4a and b *alone* do not allow to definitely make a decision between possibly existing flux flow or Ohmic resistances current limiting, respectively. Stability functions

have to be checked (Section 4.1) whether besides control of temperature fields this additional method could be necessary and sufficient to identify the physical origin of current limitation.

When instead of random values of T_{Crit}, J_{Crit}, $B_{Crit,1}$ and $B_{Crit,2}$ a set of variables is used that apart from their individual field or temperature dependency would be *identical*
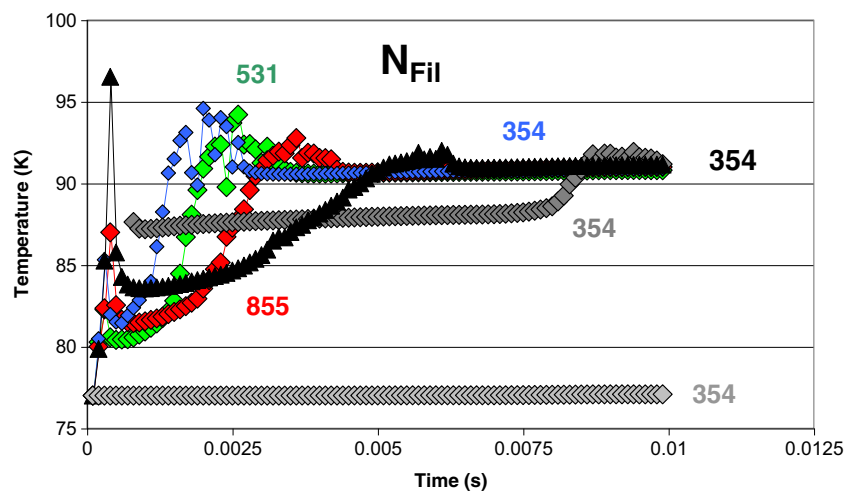
**Fig. 6** Element temperature, $T(x, y, t)$, calculated at an axial distance of 100 μm from the lower end of the short conductor section at positions close to the superconductor/matrix interface, for different numbers, N_{Fil}, of identical filaments switched in parallel, then in series, to the normal conductor. *Coloured symbols* apply L_{SC} = 5000 m and L_{Cu} = 10^3 m and the higher J_{Crit}. *Solid black triangles* apply L_{SC} = 500, L_{Cu} = 10^4 m and the higher J_{Crit}; *solid light* or *dark grey diamonds* refer to the flux flow limiter design of [4], with L_{SC} = 232 m, L_{Cu} = 4.2 10^4 m and the lower and higher J_{Crit}, respectively. All results have been calculated using a divisor, $N_{Cut\,off}$ = 20 (final value), and *random* critical variables that are different in each element (but with the same field or temperature dependency)

in each element, we obtain a very regular, stratified temperature distribution (Fig. 5). Accordingly, the variations seen in Fig. 4a, b might be the consequence of using random T_{Crit}, J_{Crit}, $B_{Crit,1}$ and $B_{Crit,2}$. Since these were intended to account for deviations from ideal conductor properties, the well-known hot spot problem in first-generation HTSC (prepared by the OPIT method) might be explained by statistical variations of conductor materials quality or from tolerances in production processes.

An example for excursion of local conductor (element) temperature, $T(x, y, t)$, with time is shown in Fig. 6 for a different number N_{Fil} of identical filaments. After the first 3 ms of the simulation (a numerical settling procedure, with fluctuations from numerical instabilities), element temperatures gradually converge to values near critical temperature to obtain quasi-stationary, discrete states (this settling procedure is shorter than the period of time that is needed to generate bubbles at the superconductor/coolant interface,
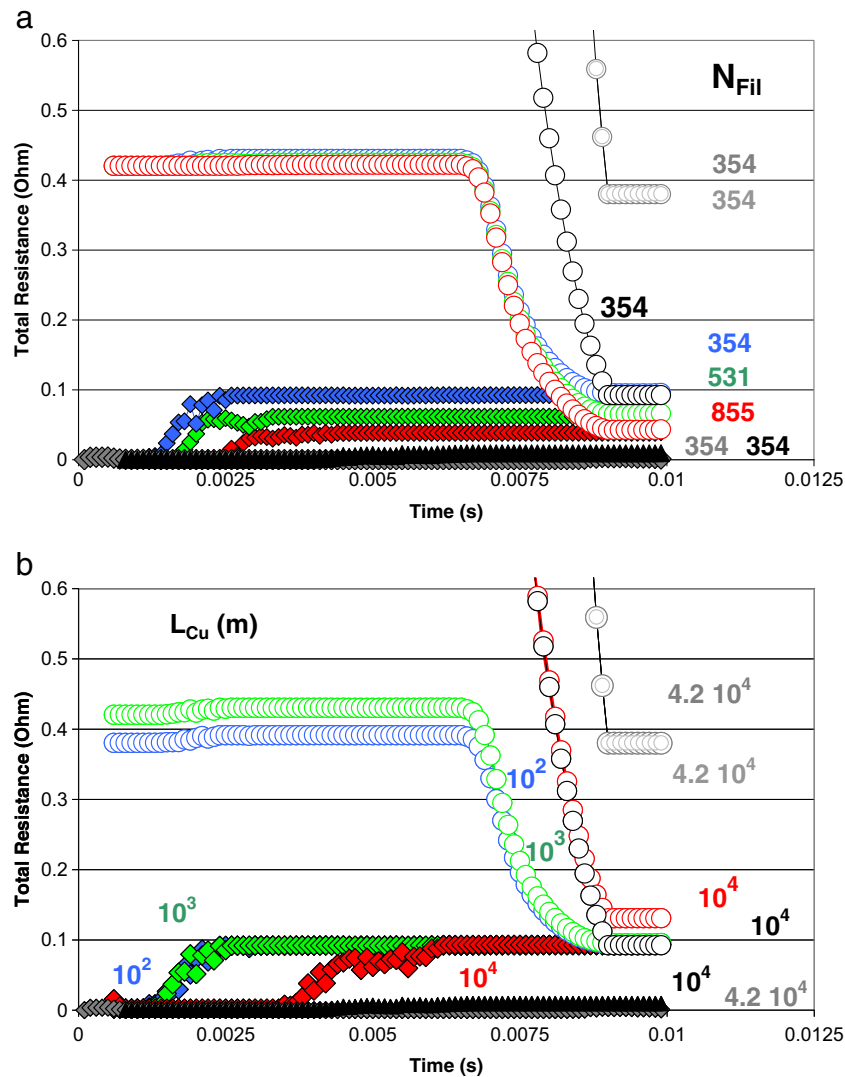
Fig. 7 a Coincidence of total (AC) phase resistance (*open coloured and light* and *dark grey circles*) and total (AC) filament resistance (*solid coloured diamonds*), for different numbers, N_{Fil}, of identical filaments. *Coloured diamonds* are calculated with $L_{SC} = 5000$ m, $L_{Cu} = 10^3$ m and the higher J_{Crit}. *Solid black triangles* apply $L_{SC} = 500$, $L_{Cu} = 10^4$ m and again the higher J_{Crit}. *Solid light or dark grey diamonds* and *circles* refer to the flux flow limiter design of [4], with $L_{SC} = 232$ m, $L_{Cu} = 4.2\ 10^4$ m and the lower and higher J_{Crit}, respectively. As before, all results are obtained with the divisor $N_{Cut\,off} = 20$ (final value) and *random*, but equally field- or temperature-dependent variables. Coincidence is obtained only

between *open* and *solid coloured symbols*. In other cases (all observed with short filament lengths), the residual phase resistance is larger than the filament resistance, and no substantial current limitation can be obtained. **b** Coincidence of total phase resistance calculated as before (Fig. 7a) but for different lengths, L_{Cu}, of the normal conductor in the phase (initiating different current loads) and with constant number, $N_{Fil} = 354$, of identical filaments. *Coloured solid* and *open symbols* apply to $L_{SC} = 5000$ m, $L_{Cu} = 10^2$, 10^3 or 10^4 m and the higher J_{Crit}. Coincidence is obtained only with the higher loads (permitted by the smaller L_{Cu}) onto the filaments

to justify modelling heat transfer to the coolant across a smooth metallic surface under static conditions).

3.2 Phase and Filament Resistances

Figure 7a, b shows how total (AC) *phase* resistance and total (AC) *filament* resistance develop with time, for different numbers of filaments and different lengths of filaments and normal conductor, respectively.

In Fig. 7a, coloured open symbols (the final total resistance of the phase) coincide with total filament resistances if $L_{SC} = 5000$ m (coloured diamonds). This indicates that only in this case will filament resistances finally become responsible for the residual total resistance of this phase. Such coincidence is not observed for shorter conductor lengths ($L_{SC} = 500$ m, or for the system described in [4], with $L_{SC} = 232$ m only). In these cases, the residual phase resistance still is larger than the corresponding filament resistance. No efficient current limitation can be expected if current limiter resistance is much smaller than the total residual phase resistance.

The same calculation is performed (Fig. 7b) with a constant N_{Fil} but a different load on the filaments initiated by different lengths L_{Cu} that specify current load on the filaments. No coincidence is obtained if $L_{Cu} \geq 10^4$ m.

In summary of Fig. 7a, b, total phase resistance only then results from overwhelming total filament resistance if their length is at least $L_{SC} = 5000$ m and if there is a higher current load which requests L_{Cu} below 10^4 m (the current load is shown in Fig. 8).

It is obvious from Fig. 7a, b that the onset of a fault current at $t = 6.5$ ms is not reflected by a corresponding increase of calculated filament resistances. The fault current does not (or does not sufficiently) trigger a substantial reaction of the filaments. Instead, it is the filament resistance that exists from the *beginning* of the simulations to which the total phase resistance converges finally. This indicates there might be Ohmic losses over all this period, not only after a fault has been initiated.

Absence of a triggering signal also concerns the design of [4]: When using the lower J_{Crit}, the conductor temperature in Fig. 6 (light grey diamonds) remains very close to 77 K. When instead using, for the same design, the higher J_{Crit} (dark grey diamonds), a substantial increase of conductor temperature is not observed before $t \geq 7.5$ ms. Filament resistances generated by concept [4] are too small, at least under the small current load (L_{Cu} very large, $4.2 \ 10^4$ m, needed to replicate the assumed permanent impedance of $0.38 \ \Omega$) to compensate reduction of total phase resistance.

Can substantial current limitation be obtained with concept [4] if the load would be increased? By assuming reduced lengths L_{Cu} of the normal conductor below 10^4 m?

The answer can be given from inspection of the solid black triangles in Figs. 6 and 7b: (a) The conductor temperature in Fig. 6 is driven close to or above critical temperature, which means the limiting concept no longer relies on flux flow but mostly on Ohmic resistances, and (b) total filament resistance in Fig. 7b still would be too small to coincide with the total phase resistance.
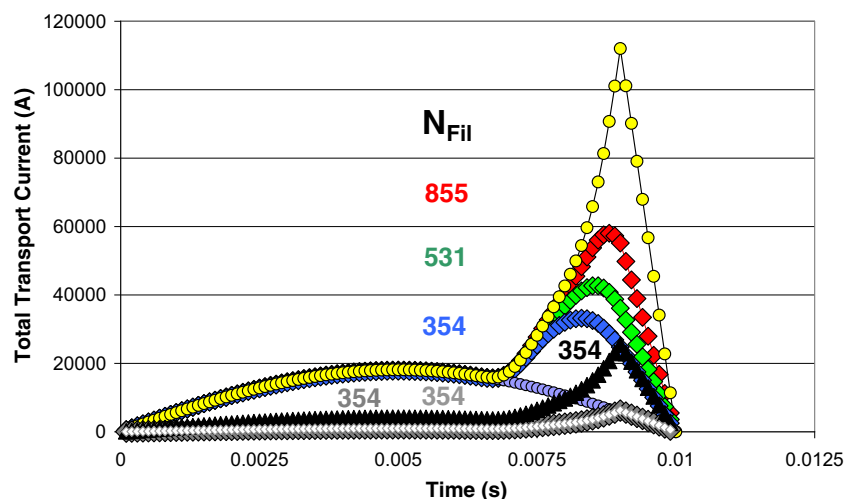
Fig. 8 Total (nominal plus fault) current for different numbers, N_{Fil}, of identical filaments (*solid coloured diamonds*) calculated using $L_{SC} = 5000$ m, $L_{Cu} = 10^3$ m and the higher J_{Crit}. *Solid black triangles* apply $L_{SC} = 500$, $L_{Cu} = 10^4$ m and again the higher J_{Crit}. *Solid light* or *dark grey diamonds* refer to the flux flow limiter design of [4], with $L_{SC} = 232$ m, $L_{Cu} = 4.2 \ 10^4$ m and the lower and higher J_{Crit}. *Solid lilac circles* denote transport current if there is no

superconductor and no disturbance (no short circuit or the like) of the normal conductor, while *solid yellow circles* indicate current with no superconductor but with the disturbance of the normal conductor initiated by the $N_{Cut\,off}$. The *sharp peak* of the *yellow circles* and of the *solid black triangles* results from the discrete time steps in the simulations. All results have been obtained with *random* (but equally field- or temperature-dependent) critical variables

A second attempt might be more successful: Length L_{SC} of the filaments (232 m in concept [4]) could be increased. But the black triangles in Fig. 6 indicate an increase to $L_{SC} = 500$ m would not be sufficient while an increase to $L_{SC} = 5000$ m would early drive conductor temperature out of the flux flow regime (coloured diamonds in Fig. 6). Accordingly, it is not clear that substantial limitation could practically be achieved with flux flow resistive conductor states; a thorough re-design becomes necessary.

Shimizu et al. [4] assume that the FCL *instantly*, at the very beginning of a fault, generates a resistance (and would also be able to pass a load current immediately after fault clearing). At least the first assumption is questionable (compare again the *gradual* increase of element temperature in Fig. 6, solid dark grey diamonds and solid black triangles).

3.3 Residual Total Current

The total phase current (nominal transport plus fault currents), calculated from nominal system voltage and from the total phase resistances (Fig. 7a, b), is shown in Fig. 8. This figure also shows excursion of current if (a) there is no superconductor and no disturbance (no short circuit or the like) of the normal conductor (solid lilac circles) while (b) solid yellow circles indicate a current with no superconductor but with the disturbance of the normal conductor.

In medium voltage distribution systems, traditional power switches (vacuum interrupters) are assessed to 12 to 24 kV, rated current 4000 A and rated short circuit breaking current of 60 kA. The current peak (yellow circles in Fig. 8) is higher, more than 120 kA, but is within range of fault currents that in medium voltage electrical systems may arise (up to 250 kA if there is absolutely no current limitation). Short circuits presently are handled by conventional current (I_s) limiters. Without protection, no electrical, medium voltage system could physically withstand this load, even within the shortest periods of time.

Accordingly, it is *this* extreme case (yellow circles in Fig. 8) to which the results obtained for the total limited current (coloured diamonds) have to be compared. In the other cases (black triangles, light and dark grey diamonds), a comparison has to be made with respect to the corresponding peaked curves.

From comparison of the different curves in Fig. 8, the filaments indeed provide substantial reduction of the total (nominal and fault) current, without runaway of their temperature, but a *direct* response to the simulated fault circuit, at a specific time t' after onset of the fault ($t \geq 6.5$ ms), cannot be identified. Instead, if we neglect an initial settling period, it seems limitation is achieved by the filaments from the beginning, $t = t_0$, of the simulations. But a limitation is clearly seen and will explicitly be shown later (Fig. 11).

As final conclusions of Section 3, when using a bundle of filaments and a model conductor, the properties of which are not too far away from conductors in technically realised devices, we see that (a) conductor temperature and, accordingly, critical and transport current distribution in these filaments are not homogeneous and (b) efficient fault current limitation, by *solely* flux flow resistance, is hard to achieve. The amount of current limiting by the filaments is clearly evident, but a sudden increase of filament resistance triggered by onset of a fault cannot be identified.

4 Stability and Correlation with Current Limiting

4.1 Stability Functions

Though it appears current limitation by phase change is observed in Figs. 7a, b and 8, a safe decision upon the real limitation mechanism (Ohmic or from flux flow resistance) cannot be made up to this point.

In this section, we will check whether stability functions, an integral view of critical current density distributions, or stability functions *plus* temperature fields, could provide this information. If it is clear that current limitation is solely by Ohmic resistances, stability functions reflect temperature distribution, $T(x,y,t)$, in the conductor. For example, oscillating temperature profiles should be reflected by corresponding oscillations of the stability function, as was observed in [10, 11].

Experimental investigations of J_{Crit} of high-temperature superconductors (compare the original literature cited in [9]) proved the relation between critical current density and temperature

$$J_{Crit}(T) = J_{Crit0}[1 - T/T_{Crit}]^n \qquad (3a)$$

is applicable also to these materials if an exponent $n = 2$ is applied. To take into account the dependence of J_{Crit} on also the local magnetic field (flux flow density, B), we apply as an approximation a standard relation

$$J_{Crit}(T, B) = J_{Crit}(T)/(B_0 + B(t)) \qquad (3b)$$

with local $B(t)$ and B_0 a constant.

The stability function, $\Phi(t)$, originally assumes critical current density to solely depend on conductor temperature. In this case, there are non-zero contributions to the stability integral

$$0 \leq \Phi(t) = 1 - \int J_{Crit}(x, y, t)dA / \int J_{Crit}(x, y, t_0)dA \leq 1 \qquad (4a)$$

only if element temperature $T(x, y, t) < T_{Crit}(x, y, t)$; otherwise, $J_{Crit}(x, y, t)$ is zero. Equation 4a is approximated by

$$0 \leq \Phi(t) = 1 - \Sigma J_{Crit}(x, y, t)dA / \Sigma J_{Crit}(x, y, t_0)dA \leq 1 \tag{4b}$$

The summations are taken over all superconductor elements in planes y= const; the result is summed up over all planes and finally divided by the total number of planes in the conductor. The result is the stability function averaged over conductor volume. The differential dA in (4b) denotes finite element cross section.

The stability function assumes values $0 \leq \Phi(t) \leq 1$ of which $\Phi(t) = 0$ are the optimum and $\Phi(t) = 1$ the worst case. Time $t_0 = 0$ denotes the start of the present simulation; at this time, all element temperatures are at their original values, $T(x, y, t_0) = 77$ K, and critical current density, $J_{Crit}(x, y, t_0)$, is maximum. Its distribution at t_0 accordingly is homogeneous, apart from statistical fluctuations caused by the random J_{Crit0} (the materials property). This situation quickly changes at times $t > t_0$.

In previous stability calculations [8–11], in (4a, 4b), only the dependence of J_{Crit} on temperature was considered; calculations were performed for standard disturbances. These were not induced by a nominal transport or fault current but were of the familiar type, like transformation of mechanical stress energy to thermal energy, absorption of particle radiation or the like. In the present paper, however, we have to apply temperature *and* field dependence of J_{Crit} for calculation of stability functions because $J > J_{Crit}$, too, constitutes a disturbance, by flux flow losses. A problem then arises from application of (4a, 4b):

When assuming flux flow resistive conditions, the conductor temperature is below critical temperature, which means integrals or summations in (4a, 4b) might apply values of $J_{Crit}(x, y, t)$ close to $J_{Crit}(x, y, t_0)$. Stability function Φ then is small, and maximum zero-loss transport current

$$I_{max}(t) = J_{Crit}[T(x, y, t = t_0)][1 - \Phi(t)]A_{SC} \tag{5}$$

is close to $I_{max}(t_0)$, with A_{SC} the total conductor cross section.

But flux flow resistances and corresponding losses are not directly correlated with conductor temperature; there is at best a correlation with temperature indirectly by the temperature dependence of normal conduction resistivity, ρ_{NC}, in (1). Only the condition $T < T_{Crit}$, at all times, t, has to be fulfilled. Thus, flux flow losses are correlated neither with values J_{Crit} nor with Φ. Stability function Φ and maximum zero-loss current, $I_{max}(t)$, accordingly can reasonably be

calculated from (4a, 4b) and (5) only for Ohmic resistance states (as was done in [8–11]) or, approximately, if there are only few elements that show flux flow resistance. If flux flow resistance would strongly contribute to total resistance, the procedure using (4a, 4b) and (5) is no longer applicable.

This is illustrated in Fig. 9 that shows stability functions for a different number of filaments. In all cases, the dependence of (random) J_{Crit} on temperature and magnetic fields has tentatively been applied to (4a, 4b). Under small magnetic fields, as is mostly the case in the present simulations, the difference between $J_{Crit}(T)$ and $J_{Crit}(T, B)$ is small. The obtained Φ thus are very close to 1 since the $T(x, y, t)$ are close to or exceed $T_{Crit}(x, y, t)$. The large Φ indicate that indeed only few elements are at temperatures below T_{Crit}; in other words, an overall phase change to normal Ohmic resistance states has occurred, with little contribution of flux flow to total resistance. The application of (4a, 4b) and (5) thus was justified.

Though it appears at first sight that it is only a theoretical discipline, the following relations shall be checked whether they would provide benefits of practical interest.

(1) Given $T(x, y, t) > T_{Crit}(x, y, t)$, then $J_{Crit} = 0$ and $\Phi = 1$. This is clear from the previous comments (and is the natural way of operation of an Ohmic resistive FCL). Check whether the reverse (1′) of (1) is true:

(1′) From Φ close to 1, we cannot uniquely conclude $T > T_{Crit}$. Given a large transport current, it might create a sufficiently large magnetic field that at sufficiently high temperature, in particular if it is close to critical temperature, exceeds $B_{Crit,2}(T) = B_{Crit,2}(x, y, t)$, with $T = T(x, y, t)$. Accordingly, the reverse relation (1′) to (1) "If is close to 1 (which means the $J_{Crit}(x, y, t)$ are close to zero), then $T(x,y,t) > T_{Crit}(x,y,t)$", holds *only* if the magnetic field is small against $B_{Crit,2}(x, y, t)$. In the present simulations, local $B(x, y, t)$ fulfil the condition $B(x, y, t) << B_{Crit,2}(x, y, t)$ except for temperatures very close to the critical temperature. This means that under the condition "$B(x,y,t)$ small", the reverse (1′) is true. We have a logically, bijectively connected correlation between stability, critical current density and temperature.

The large Φ observed in Fig. 9 accordingly indicates that element temperature, in a very large fraction of the superconductor volume, is above critical temperature (the result already seen in Fig. 4b). This conclusion is also correct in case of the design in [4], but only for $t > 8$ ms, and the stability function in Fig. 9 (dark grey diamonds) is plotted for this period only.

The question then is whether a bijective correlation exists also between superconductor stability and current limiting. What can we learn for superconductor safety if such a correlation would *not* exist?
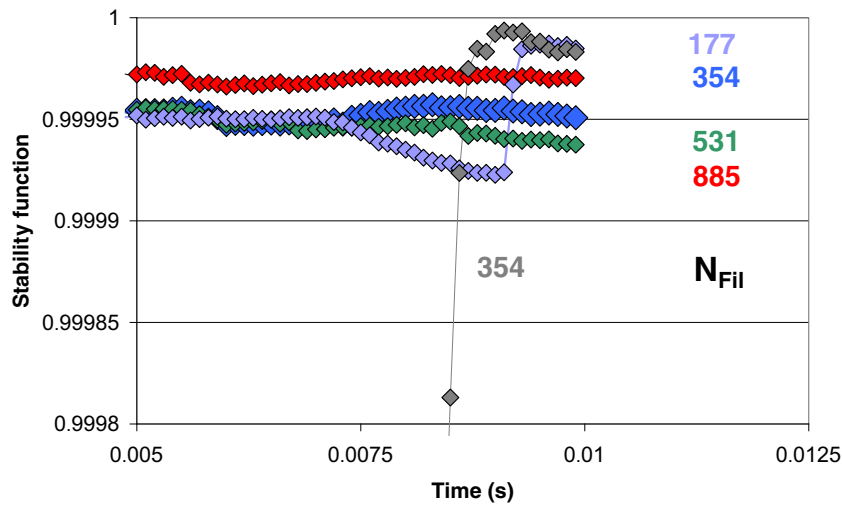
Fig. 9 Volume averaged stability functions, within $5 \leq t \leq 10$ ms, for different numbers, N_{Fil}, of identical filaments. *Coloured diamonds* apply $L_{SC} = 5000$ m, $L_{Cu} = 10^3$ m and the higher J_{Crit}. Scattering of the data results from the random J_{Crit0} (the materials properties). *Solid dark grey diamonds* refer to $L_{SC} = 232$ m, $L_{Cu} = 4.2\ 10^4$ m, $N_{Fil} = 354$ (the flux flow limiter design of [4]) and the *higher* J_{Crit} (this curve reasonably can be calculated only for $t > 8$ ms; compare text). Results

obtained with the same L_{SC}, L_{Cu} and N_{Fil}, but with the *lower* J_{Crit}, are not shown (the stability function again cannot be applied; if yet a formal calculation is performed, the stability function at all $t \leq 10$ ms, with very small variations amounts on the average to 0.65, the average taken over six planes located at the same axial positions as the J_{Crit} in Figs. 5b and 10)

4.2 Correlation of Stability with Current Limiting

Distribution of critical current density, $J_{Crit}(T, B)$, for the flux flow resistance limiter design [4], calculated with the *lower* J_{Crit}, is shown in Fig. 10. The almost homogeneous distribution reflects the homogeneous temperature field in Fig. 4a (temperature variation within 0.5 K) and Fig. 6 (light grey diamonds). The stability function, if again tentatively calculated with an extension of (4a, 4b) to also include the dependence of $J_{Crit}(x, y, t)$ on $B(x, y, t)$,

$$0 \leq \Phi(t) = 1 - \int J_{Crit}[T(x, y, t), B(x, y, t)] dA / $$
$$\int J_{Crit}[T(x, y, t_0), B(x, y, t_0)] dA \leq 1 \qquad (6)$$

depends on ratios $J_{Crit}(t)/J_{Crit}(t_0)$, with $J_{Crit}(t_0) = 10^7$ A/m^2 ("tentatively" means before it is clarified that there are only or strongly dominating Ohmic resistance states). Apart from statistical fluctuations, these ratios closely approach unity, and the stability function accordingly should be small.

A limitation factor Ψ shall be defined as the ratio between absolutely unlimited total (nominal plus fault) current to total limited current. In Section 4.3, this concerns a comparison between solid yellow circles and solid coloured diamonds, and between black triangles and grey diamonds with the corresponding peaked curves. Note that Fig. 11 shows Ψ in dependence on L_{Cu} (Ψ is given for a different current load onto the filaments), not the dependence of Ψ on L_{SC}.

Fig. 10 Distribution of critical current density in a superconductor filament, calculated at $t = 9$ ms after the start of the simulation (the end of the increase of $N_{Cut off}(t)$) using $L_{Cu} = 4.2\ 10^4$ m, $L_{SC} = 232$ m and $N_{Fil} = 354$ (the design reported in [4]) with the lower J_{Crit}. Axial positions (distances from the lower end of the conductor section) indicated by *blue*, *red*, *dark green*, *light green*, *dark yellow* and *lilac* diamonds are 0.1, 0.7, 1.3, 1.9, 2.5 and 3.1 mm, respectively
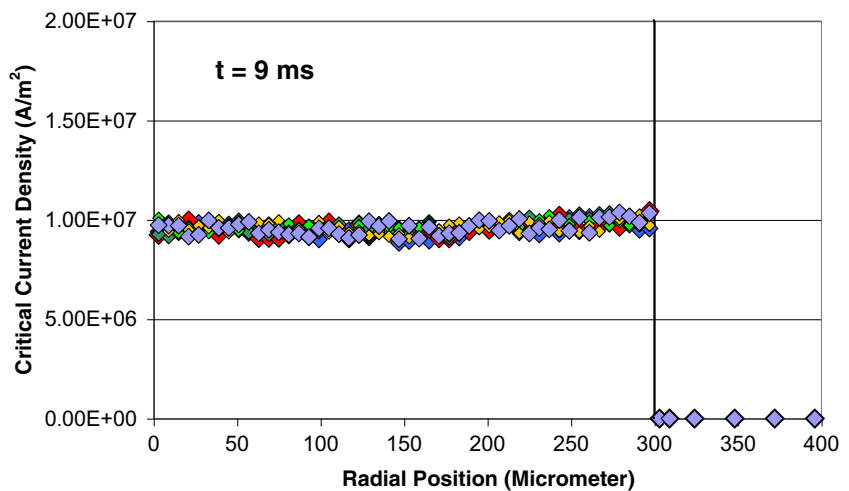
(2) Given $\Phi = 1$, then $J_{Crit}(x, y, t) = 0$, and $T(x, y, t) > T_{Crit}(x, y, t)$ and Ψ are accordingly large. Again, this correlation is clear from the previous comments. Check whether the reverse (2′) or (2″) is true: Given large Ψ, how large is Φ?

(2′) Substantial current limiting, Ψ, can be achieved if the conductor length, L_{SC}, is strongly increased, or the conductor cross section, A_{SC}, is made sufficiently small. All this does not alter J_{Crit0}, a materials property, and accordingly does not alter Φ, if it is tentatively calculated from (6), and for small $B(x, y, t)$. Strong current limiting, Ψ, then either suggests $T(x, y, t) > T_{Crit}(x, y, t)$ that yields $J_{Crit}(x, y, t) = 0$ and $\Phi = 1$ (a first extreme case) or, under variation of conductor dimension (large L_{SC}, small A_{SC}) and $T(x, y, t) < T_{Crit}(x, y, t)$, it suggests $\Phi \to 0$, the other extreme case. This means: Contrary to (1) and (1′), a correlation (2) and (2′) is not bijective.

Inspection of solely Ψ, if one does not know anything about $J_{Crit}(T, B)$, with $T = T(x, y, t)$ and $B = B(x, y, t)$, also does not allow a decision (2″): It is not clear that the device would be stable against quench. Given large Ψ, how large is Φ? Is the device stable?

(2″) Large Ψ can be obtained with large L_{SC} and small A_{SC} (large conductor resistance). The conductor temperature shall be below but possibly close to T_{Crit} (most of the conductor cross section in flux flow, but a considerable part in Ohmic resistive states). In this case, flux flow resistance or Ohmic losses might quickly drive the temperature beyond this limit (compare the solid dark grey symbols in Fig. 6). Thus, a correlation also between (2) and (2″) is not bijective. This implies little stability of the device. Under practical aspects, serious consequences for conductor safety would arise if temperature and field distribution is not controlled in parallel to the control of Ψ.

Finally, it would be interesting to check whether the propagation velocity of a normal zone in YBaCuO cables as reported in [23], in relation to a propagation of the temperature front, both calculated with a finite element method, can be explained by a similar correlation analysis as presented above, and whether inhomogeneities and current percolation have been observed. This will be investigated in a separate paper.

4.3 Limitation Factors

Limitation factors, Ψ, to fault current can be extracted in Fig. 11 from the ratio between solid yellow circles and coloured diamonds for long conductor lengths, $L_{SC} = 5000$ m, and for short conductor lengths, $L_{SC} = 500$ m (solid black triangles) or $L_{SC} = 232$ m (light grey diamonds, the flux flow limiter design of [4]). A modest limitation is observed: The total unlimited current (solid yellow circles) is reduced by about a factor $\Psi \leq 5$ to the total limited current. This result is achieved with the larger conductor lengths. The reduction of unlimited fault current is the higher the larger the load (the fault current) onto the filaments. For the short conductor length, no substantial limitation is observed.

5 Summary

If besides standard disturbances (like release of mechanical energy) the transport current itself constitutes disturbances, the determination of local temperature *and* of local current distribution becomes mandatory. This is necessary to appropriately handle stability models and for making a step forward to conclude under which resistance states (Ohmic or flux flow) current propagation would be limited.

Temperature profiles observed in this paper, with variations ΔT up to about 7 K, do not allow a clear distinction between Ohmic resistive or flux flow resistive fault current limiting concepts. Though frequently made in the literature, this separation is highly questionable. Ohmic resistive and flux flow resistive states may locally coexist, side by side, but are not very stable in conductor volume.

The magnitude of the nominal plus fault current may fluctuate in the interior and percolate through a polycrystalline, porous conductor by a network of grains and grain boundaries.

Any superconductor, even if perfectly designed and manufactured with highest available precision, over extended lengths in reality never will exhibit perfectly homogeneous materials properties. An attempt has been made in this paper to account for this problem by means of a random variation of the most important conductor materials properties; it is a potentially new method to improve the safety of electrical circuits incorporating superconducting components and reliability of stability predictions, but additional work is required to verify this concept with different superconductor materials and conductor architectures.

Unique (bijective) correlations cannot be found between stability and current limiting if there is flux flow resistivity, which probably constitutes a safety problem for all cases of current propagation when the transport current exceeds critical current density.

Appendix A1: Definition of Model Conductor and Conductor Architecture

For convergence of the numerical simulations, we need a combination of

(A) Superconductor material, all properties of which are suitable for finite element simulations of local, transient thermal states and current propagation

(B) Simple conductor architecture with preferentially cylindrical symmetry and, in case of HTSC, and as far as possible, c-axis orientation of the superconductor

As a straight-ahead selection of conductor material and conductor architecture, a combination of BSCCO material with powder in tube (OPIT) 1G (first-generation) conductor architecture apparently would be the ideal situation, with technically realised 1G conductors immediately at hand. While this selection conforms with *manufacture* issues, it is not very suitable for numerical simulations of conductor stability. Though the missing weak-link problem would be favourable for the modelling of current transport, the anisotropy of BSCCO is too large, in the order of 10^3, to yield convergence of the simulated results. Numerical stability analysis of the proper 1G conductor using BSCCO thus is not possible.

Concerning solely *materials* properties, the situation is better with YBaCuO (anisotropy in the order of 10). Thermal diffusivity of this material is available from 77 to 600 K (to include also resistive states); otherwise, convergence problems again would be expected. But YBaCuO is not very suitable for standard metallurgy (powder in tube) preparation steps. The material is too hard and brittle; many cracks would be the consequence. An efficient texture is not achievable with this technique, and there is also the weak-link problem in this material.

Similar convergence problems come up in simulations of a 2G conductor: The large number of components involved, a series of thin films, with strongly differing mechanical/thermal properties and thicknesses constitutes a simulation problem that finite element schemes do not like at all. There would be a lot of interfaces between the single layers of which, strictly speaking, absolutely no reliable quantitative information on corresponding thermal contact resistances is available.

Instead, a *model* conductor has been applied in the calculations to circumvent both convergence problems and manufacture concerns. The electrical/magnetic and thermal properties of the model conductor shall allow generally valid, qualitative conclusions on possibly existing inhomogeneity within the conductor cross section of temperature and current distribution and of the distribution of the other properties and parameters mentioned in Section 1.

The model conductor consists of a bundle of YBaCuO filaments integrated into a metallic matrix and with a statistical variation of its most important materials properties. Presently, only this combination of HTSC material and conductor architecture can be applied for numerical analysis of current propagation in general, and of current limiting. While preparation of $YBa_2Cu_4O_8$ and $YBa_2Cu_3O_{7-\delta}$ multi-filamentary wires hardly could be realised with OPIT, the situation is better with the metal precursor technique described in [24] and, for one possible direction of its development, [25], respectively. Although its cross section resembles a 1G conductor, the model conductor is *not* of the proper 1G type since it does not contain BSCCO as the
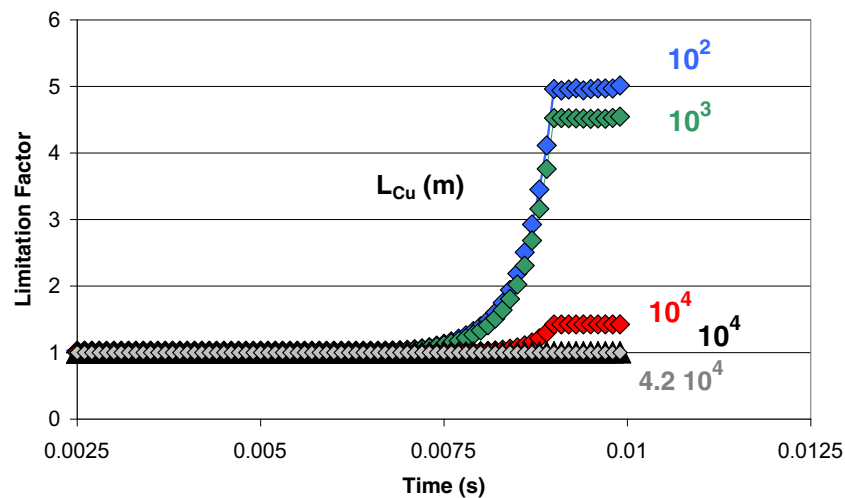
Fig. 11 Limitation factor (damping), Ψ, the ratio of total (nominal plus fault) unlimited current to limited current, obtained with $N_{Fil} = 354$ superconducting filaments, all switched in parallel and in series to the normal conductor. Results refer to different lengths, L_{Cu} (different current loads onto the filaments), of the normal conductor (*coloured diamonds*); these are obtained with $L_{SC} = 5000$ m and the higher J_{Crit}. *Solid black triangles* apply $L_{SC} = 500$, $L_{Cu} = 10^4$ m and the higher J_{Crit}. *Solid light grey diamonds* refer to the flux flow limiter design of [4], with $L_{SC} = 232$ m, $L_{Cu} = 4.2\ 10^4$ m and the lower J_{Crit} (application of the higher J_{Crit} coincides with the *light grey symbols*). Substantial current limitation (Ψ about ≥ 2) is observed only with the shorter normal conductor lengths (increased load onto the filaments)
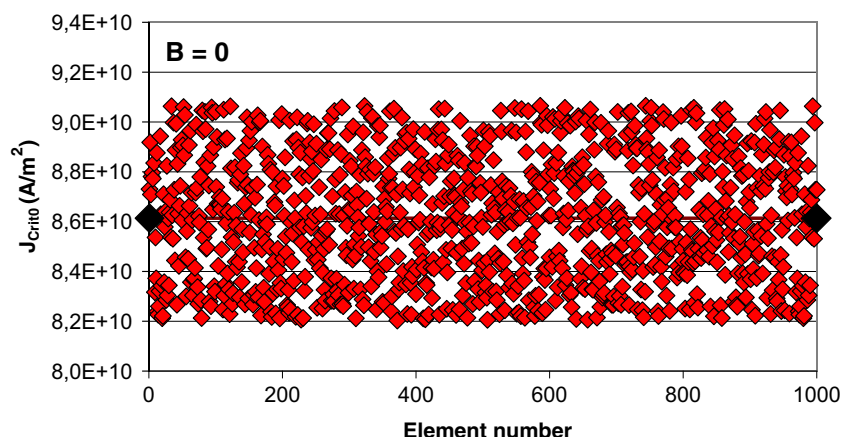
Fig. 12 Random reference values, J_{Crit0} (materials properties) used for calculation of the higher critical current density, $J_{Crit}(T, B)$, then with its dependence on local temperature, T, and on local magnetic field (magnetic flux density), B. *Solid black diamonds* connected by the *solid horizontal black line* indicate arithmetic mean,

$J_{Crit0,m} = 8.614 \ 10^{10}$ A/m². When using $T = 77$ K, $T_{Crit} = 92$ K, $B_0 = 6$ T and $B = 100$ mT, we have $J_{Crit}(T, B) = J_{Crit0,m} \ 10^{10}$ $(1 - T/T_{Crit})^2/(B_0 + B) = 3.75 \ 10^8$ A/m² referenced as the higher J_{Crit} in the text and figure captions

standard material for the superconducting core. It is simply a conductor that is suitable for a systematic study of current propagation but the results are representative for also other superconductor materials and architectures.

Thermal conductivity, specific heat of the model conductor and density (after a correction to porosity) thus are the same as used in previous work; see citation in the text. Random reference values J_{Crit0} and T_{Crit0} for calculation of $J_{Crit}(x, y, t)$ and $T_{Crit}(x, y, t)$ are shown in Figs. 12 and 13 as examples. The upper and lower critical field (mean values, again of a random distribution) is 90 T and 10 mT, respectively, at 77 K. Parameters for the metallic matrix of each filament are those of Ag taken from [20], but the simulations could apply also other matrix metals, like Cu or alloys Y-Cu.

Appendix A2: Current Percolation and Sharing

The results shown in Figs. 14, 15 and 16 refer to the design [4]: $L_{SC} = 232$ m, $N_{Fil} = 354$, but the higher J_{Crit}, compare Fig. 6, and $L_{Cu} = 4.2 \ 10^4$ m (to provide in the present model an equivalent to the reported impedance of 0.38 Ω). The curves indicate total (nominal plus fault) current through the elements. Current can be taken by solely the superconductor elements at radial positions between 250 and 300 μm, and between 225 and 300 μm, at $t = 3$ and 6 ms, respectively, with successively reduced magnitude (Figs. 14 and 15; this illustrates current *percolation*). This is no longer fulfilled at $t = 9$ ms (Fig. 16) where almost all current is directed to the metallic matrix (this illustrates current *sharing*). This is in agreement with the upturn of element temperature at

Fig. 13 Random reference values of critical temperature, T_{Crit0} (again materials properties) at zero magnetic field. Data are given for a sample of 1000 elements. *Solid black diamonds* and the *black horizontal line* indicate the arithmetic mean. Like J_{Crit0} (Fig. 12), also T_{Crit0} is subsequently converted to a local dependence yielding $T_{Crit} = T_{Crit}(B)$, with $B = B(x, y, t)$
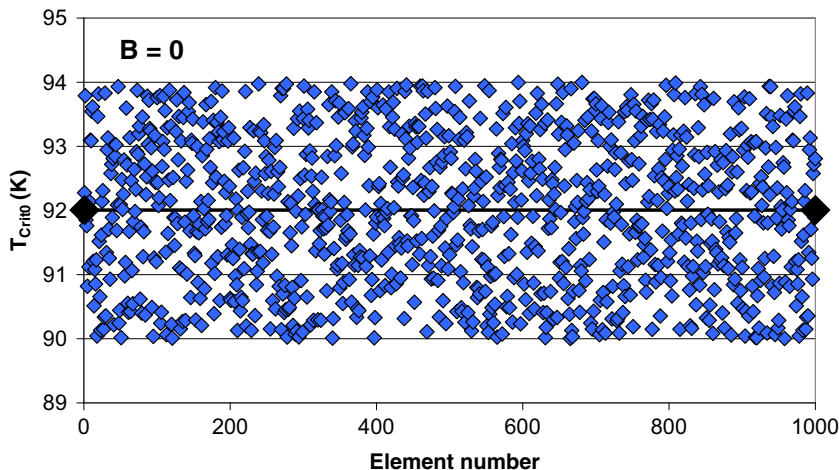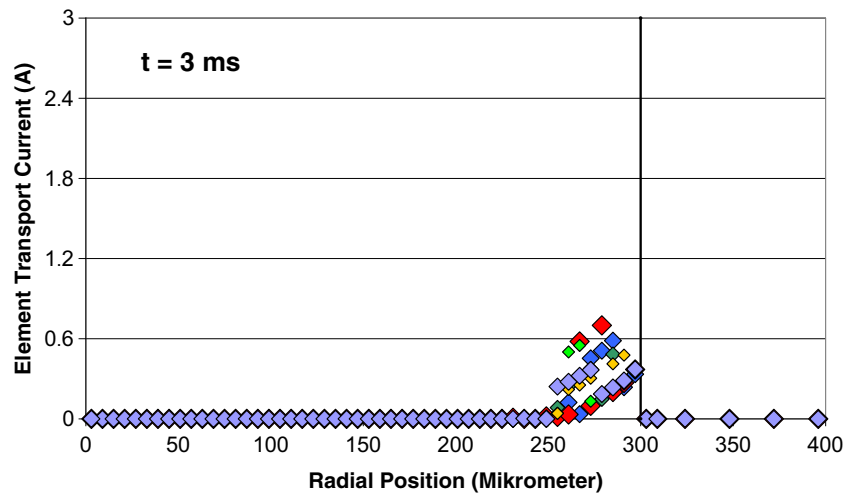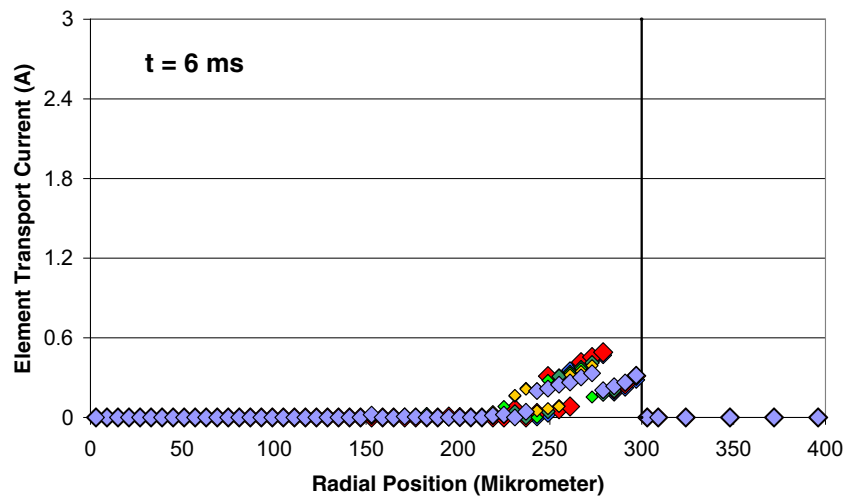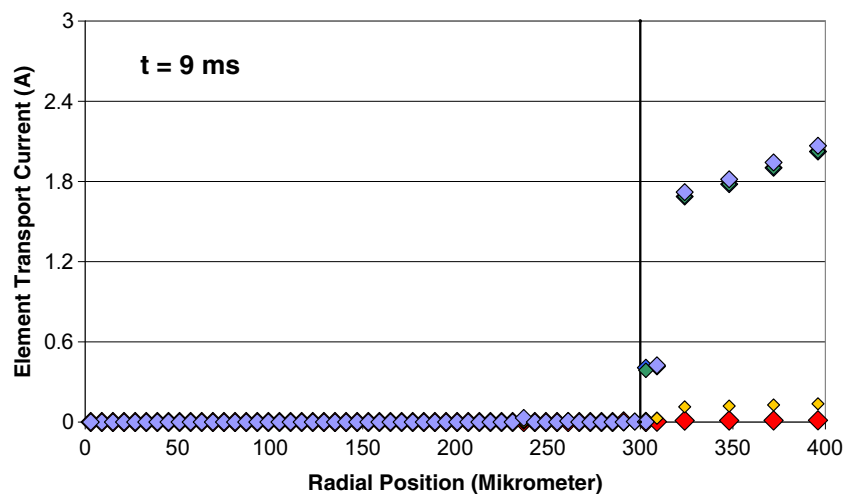
Fig. 14 Distribution of total (nominal plus fault) current in the superconductor filament and its matrix, calculated at $t = 3$ ms after the start of the simulation (before onset of the disturbance), in dependence of radial and axial positions in the conductor section. Results are calculated using $L_{Cu} = 4.2 \, 10^4$ m, $L_{SC} = 232$ m, $N_{Fil} = 354$ and the higher J_{Crit}. Axial positions (distances from the lower end of the conductor section) are indicated by *blue*, *red*, *dark green*, *light green*, *dark yellow* and *lilac diamonds*, which indicate distances of 0.1, 0.7, 1.3, 1.9, 2.5 and 3.1 mm, respectively. The *vertical bar* separates superconductor filament elements (*left*) from its metallic matrix elements

Fig. 15 Distribution of total (nominal plus fault) current in the superconductor and matrix, like in Fig. 14 but at $t = 6$ ms after the start of the simulation (still before onset of the disturbance). Axial element positions are the same as described in the caption of Fig. 14

Fig. 16 Distribution of total (nominal plus fault) current in the superconductor and matrix, like in Figs. 14 and 15 but at $t = 9$ ms after the start of the simulation. Element positions are the same as described in the caption of Fig. 14

Fig. 17 Distribution of total (nominal plus fault) current in the superconductor and matrix, like in Fig. 14 to 16 but using $L_{Cu} = 10^3$ m, $L_{SC} = 5000$ m, $N_{Fil} = 354$ and the higher J_{Crit}. Results are given at $t = 6$ ms after the start of the simulation (before onset of the disturbance). Axial element positions are the same as in Fig. 14
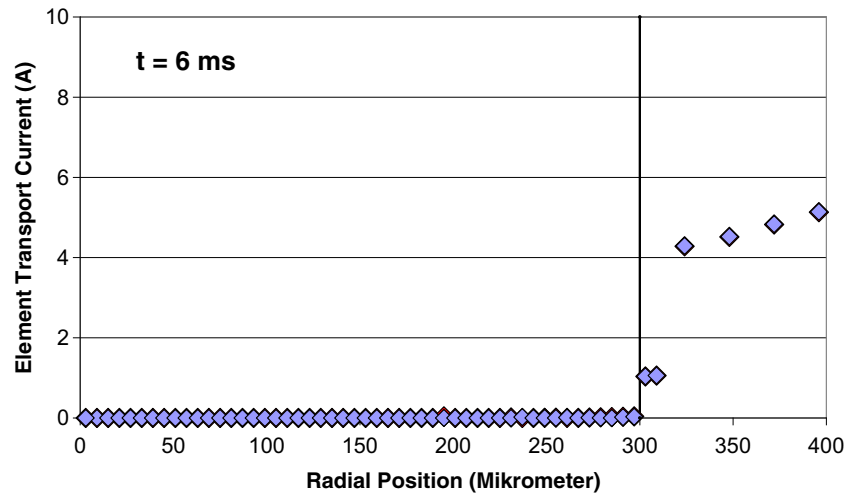
$t > 8$ ms in Fig. 6 while the decrease of sin (ωt) dependence of nominal current in this time interval is overcompensated.

The current is larger in elements located near the superconductor/matrix interface compared to the inner parts of the conductor. This confirms an early expectation [26], p. 374 (in the context of Fig. 8 of this reference): High J_{Crit} regions should be confined to the superconductor/matrix interface. The same conclusion applies to current distribution:

Experimental distribution of local critical current *densities* was in [26] correlated with the microstructure of a Bi 2223 tape. Here, we look at the alternative (but probably more informative) local distribution of *currents*, not of their densities. The distribution of critical current density does not always equal the distribution of currents: Element cross sections (concentring rings) in the present simulations increase in the radial direction (element radial width $\Delta x = 6$ mm is constant). The current will be distributed to generate losses as small as possible, i.e. it will flow preferentially in the outer elements. The homogenous distribution of critical current *density* in Fig. 10 accordingly is not reflected by a homogeneous distribution of *currents* in Figs. 14, 15, and 16.

The other example (Fig. 17) refers to $L_{Cu} = 10^3$ m, $L_{SC} = 5000$ m and $N_{Fil} = 354$, again using the higher J_{Crit}. Here, the smaller L_{Cu} strongly increases the current load (by about an order of magnitude), and a great part of element temperatures is increased above $T_{Crit}(B)$. The current is by more than 95 % directed to the matrix, not only at $t = 6$ ms.

References

1. Giese, R.F., Runde, M.: Fault-current limiters. In: Implementing Agreement for a Co-operative Programme for Assessing the Impacts of High-Temperature Superconductivity on the Electric Power Sector. Argonne National Lab., Argonne, Illinois, USA (1991)

2. Giese, R.F.: Fault-current limiters—a second look. In: Implementing Agreement for a Co-operative Programme for Assessing the Impacts of High-Temperature Superconductivity on the Electric Power Sector. Argonne National Lab., Argonne, Illinois, USA (1995)

3. Kalsi, Sw.S.: Applications of high temperature superconductors to electric power equipment, pp. 173–217. IEEE Press, John Wiley & Sons, Inc. Publ, Hoboken (2011)

4. Shimizu, H., Yokomizu, Y., Goto, M., Matsumuara, T., Murayama, N.: A study on required volume of superconducting element for flux flow resistance type fault current limiter. IEEE Transacts. Appl. Supercond. **13**, 2052–2055 (2003)

5. Sheng, J., Chen, Y., Lin, B., Ying, L., Jin, Z., Hong, Z.: Electrical-thermal-structural coupled finite element model of high temperature superconductor for resistive type fault current limiters. J. Supercond. Nov. Magn. **27**, 1353–1357 (2014)

6. Wilson, M.N.: Superconducting magnets. In: Scurlock, R.G. (ed.) Monographs on Cryogenics. reprinted paperback. Oxford University Press, New York (1989)

7. Dresner, L.: Stability of superconductors. In: Wolf, St. (ed.) Selected Topics in Superconductivity. Plenum Press, New York (1995)

8. Flik, M.L., Tien, C.L.: Intrinsic thermal stability of anisotropic thin-film superconductors. ASME Winter Ann. Meeting, Chicago, IL, Nov 29 – Dec, 2, 1988

9. Reiss, H.: Radiation heat transfer and is impact on stability against quench of a superconductor. J. Supercond. Nov. Magn. **25**(2), 339–350 (2012)

10. Reiss, H., Troitsky, O.Yu.: Superconductor stability revisited: impacts from coupled conductive and thermal radiative transfer in the solid. J. Supercond. Nov. Magn. **27**, 717– 734 (2014)

11. Reiss, H., Troitsky, O.Y.u.: Impact of radiation heat transfer on superconductor stability, Proc. 10th Intern. Workshop on Subsecond Thermophysics (IWSST), Karlsruhe, Germany (June 26 to 28, 2013), published in High Temp.- High Press., vol. 43, pp. 155–173 (2014)

12. Reiss, H., Troitsky, O.Y.u.: Radiative transfer and its impact on thermal diffusivity determined in remote sensing. In: Reimer, A. (ed.) Horizons in World Physics, vol. 276, pp 1-68 (2011)

13. Poole Jr. Ch. P., Datta, T., Farach, H.A.: Wiley, Copper Oxide Superconductors. J. & Sons, A Wiley-Intersc. Publ., New York (1988). Fig. VII –11

14. Diaz, A., Mechin, L., Berghuis, P., Evetts, J.E.: Observation of viscous flow in $YBa_2Cu_3O_{7-\delta}$ low-angle grain boundaries. Phys. Rev. B **58**(6), R2960 – R2963 (1998)

15. Huebener, R.P.: Magnetic flux structures in superconductors, Springer Series in Solid State Sciences, vol. 6. Springer-Verlag, Berlin (1979)

16. Hao, Zh., Clem, J.R.: Viscous flow motion in anisotropic type-II superconductors in low fields. IEEE Transacts. Magn. **27**, 1086–1088 (1991)

17. Gmelin, E.: Thermal properties of high temperature superconductors. In: Narlikar, A.V. (ed.): Studies of High Temperature Superconductors, vol. 2, pp. 95–127. Nova Science Publ., New York (1989)

18. Whitaker, St.: Fundamental principles of heat transfer. New York (1977)

19. Russell, H.W.: Principles of heat flow in porous insulations. J. Amer. Ceram. Soc. **18**, 1–5 (1935)

20. Smith, D.R., Fickett, F.R.: Low temperature properties of silver. J. Res. Natl. Inst. Stand. Technol. **100**, 119– 171 (1995)

21. Reiss, H.: A microscopic model of superconductor stability. J. Supercond. Nov. Magn. **26**(3), 593–617 (2013)

22. Knaak, W., Klemt, E., Sommer, M., Abeln, A., Reiss, H.: Final report (in German): Entwicklung von wechselstromtauglichen Supraleitern mit hohen Übergangstemperaturen für die Energietechnik, Bundesministerium für Forschung und Technologie, Forschungsvorhaben 13 N 5610 A, Abschlußbericht Asea Brown Boveri AG, Forschungszentrum Heidelberg (1994)

23. Härö, E., Järvelä, J., Stenvall, A.: Variation of quench propagation velocity in YBCO cables. J. Supercond. Nov. Magn. **28**(6), 1705–1710 (2015)

24. Chawla, N., Chawla, Kr.K.: Metal Matrix Composites, p. 100. Springer Verlag (2006)

25. Sugimoto, M., Kohno, O., Ikeno, Y., Sadakata, N., Nakagawa, M., Aoki, Sh., Tan, M., Okiai, R., Yoshida, S., Hasegawa, M., Yamanouchi, H.: Method of producing oxide superconducting cables and coils using copper alloy filament precursors. US Pat. 4,945,245 (October 23, 1990)

26. Larbalestier, D., Gurevich, A., Feldmann, D.M., Polyanskii, A.: High-T_c superconducting materials for electric power applications. Nature **244**(15), 368–377 (2001)